AGU ADVANCING EARTH AND SPACE SCIENCES

Geophysical Research Letters

RESEARCH LETTER
10.1029/2023GL105938

Evolution of Chorus Subpackets in the Earth's Magnetosphere

Huayue Chen[1], Xueyi Wang[1], Lunjin Chen[2], Yoshiharu Omura[3], Bruce T. Tsurutani[4], Yu Lin[1], and Zhiyang Xia[2]

[1]Department of Physics, Auburn University, Auburn, AL, USA, [2]William B. Hanson Center for Space Sciences, University of Texas at Dallas, Richardson, TX, USA, [3]Research Institute for Sustainable Humanosphere, Kyoto University, Kyoto, Japan, [4]Retired, Pasadena, CA, USA

Key Points:

- The source region of chorus subpackets has been observed by Van Allen Probe A
- The chorus subpackets have been investigated via the general curvilinear particle-in-cell simulation in the real-size magnetosphere
- Nonlinear physics is a dominant process in the evolution of chorus subpackets

Supporting Information:

Supporting Information may be found in the online version of this article.

Correspondence to:

H. Chen and X. Wang,
huayue_chen@foxmail.com;
wangxue@auburn.edu

Citation:

Chen, H., Wang, X., Chen, L., Omura, Y., Tsurutani, B. T., Lin, Y., & Xia, Z. (2023). Evolution of chorus subpackets in the Earth's magnetosphere. *Geophysical Research Letters*, *50*, e2023GL105938. https://doi.org/10.1029/2023GL105938

Received 14 AUG 2023
Accepted 25 OCT 2023

Abstract Chorus subpackets/subelements are the wave packets occurring at intervals of ∼10–100 msec and are suggested to play a crucial role in the formation of substructures within pulsating aurora. In this study, we investigate the evolution of subpackets from the upstream to downstream regions. Using Van Allen Probe A measurements, we have found that the frequency of the upstream subpackets increases smoothly, but that of the downstream subpackets remains almost unchanged. Through a simulation in the real-size magnetosphere, we have reproduced the subpackets with characteristics similar to those in observations, and revealed that the frequency chirping is influenced by both resonant current of electrons and wave amplitude due to nonlinear physics. Although the resonant currents in the upstream and downstream regions are comparable, the wave amplitude increases significantly during evolution, resulting in lower sweep rate in the downstream region. Our findings provide a fresh insight into the evolution of chorus subpackets.

Plain Language Summary Subpackets within chorus waves are suggested to play a significant role in producing the substructures within pulsating aurora. How does the frequency change inside subpackets is still an open question. In this study, the subpackets are found with Van Allen Probe A observation to be excited upstream of the magnetic equator, and propagate toward downstream. The frequency of subpackets increases with time in the upstream region, while it keeps almost unchanged in the downstream region. Meanwhile, a particle-in-cell simulation has been performed to study the characteristics of subpackets, and the simulation results agree well with those in observations. The frequency variation of subpackets is influenced by both resonant electrons and wave amplitude. Our study provides a clue for better understanding the nonlinear wave-particle interactions in the evolution of chorus subpackets.

1. Introduction

Chorus waves are intense and coherent whistler-mode emissions that are commonly observed in the Earth's magnetosphere (An et al., 2016; Burtis & Helliwell, 1969; Horne & Thorne, 1998; Li et al., 2009; Tsurutani & Smith, 1974; Tsurutani et al., 2009). These waves play a crucial role in regulating electron dynamics, including the acceleration of ∼100 keV electrons to relativistic energies (Miyoshi et al., 2015; Summers et al., 1998; Tsurutani & Gonzalez, 2006; Thorne et al., 2013), and the precipitation of energetic electrons to produce pulsating aurora (Miyoshi et al., 2020; Ozaki et al., 2018; Thorne et al., 2010; Tsurutani & Smith, 1974; Tsurutani et al., 2013) and microburst (Anderson & Milton, 1964; Kawamura et al., 2021; Miyoshi et al., 2015; Tsurutani et al., 2013). The spectrum of chorus waves typically exhibits a series of discrete elements (Goldstein & Tsurutani, 1984; Li et al., 2013; Lu et al., 2021), and each element is composed of ∼10–100 msec subpackets/subelements (Mourenas et al., 2022; Santolík et al., 2003; Tsurutani et al., 2009, 2020; Zhang et al., 2020a, 2020b). The subpackets have modulated amplitudes and are suggested to be an important driver of the substructures (∼10 msec) in pulsating aurora (Kataoka et al., 2012; Miyoshi et al., 2015; Ozaki et al., 2018).

One of the characteristic features of chorus element spectrum is the frequency chirping, where the frequency changes rapidly with time (Gao et al., 2022; Helliwell, 1967; Li et al., 2013). Among all spectra, the rising tone elements (with frequencies increasing with time) are the most frequently observed (Gao et al., 2014; Li et al., 2011). The chirping of rising tone elements is suggested to be triggered by the resonant current attributed by energetic electrons due to nonlinear effects (Hanzelka & Santolík, 2023; Nunn, 1974; Omura, 2021; Omura et al., 2008; Roux & Pellat, 1978; Vomvoridis et al., 1982; Zonca et al., 2022). The corresponding sweep rate, which is a key parameter depicting the rapidity of the frequency chirping, has been extensively studied in both observations (Cully et al., 2011; Macúšová et al., 2010; Tao et al., 2012) and simulations (H. Chen et al., 2022;

Katoh & Omura, 2011; Ke et al., 2020). However, the investigations on frequency chirping of subpackets are still limited (H. Chen et al., 2023a; R. Chen et al., 2022; Tsurutani et al., 2020; Zhang et al., 2020a, 2020b). It is generally believed that the frequency of subpackets within the rising tone elements would also increase (Santolík et al., 2003; Zhang et al., 2020b). However, Tsurutani et al. (2020) and R. Chen et al. (2022) examined the large amplitude subpackets, and found their frequency to be nearly constant.

The chorus source region is proposed to be near the magnetic equator (Burtis & Helliwell, 1969; Tsurutani & Smith, 1974), where the linear growth rate is at its maximum (H. Chen et al., 2022; Lu et al., 2019). However, nonlinear theory proposed that the source region of chorus subpackets is located upstream (relative to wave propagating direction) of the magnetic equator, because the resonance velocity of electrons is opposite to wave group velocity, leading to the sum velocity pointing upstream (Nogi & Omura, 2022, 2023). Via Time History of Events and Macroscale Interactions during Substorms (THEMIS) observations, Demekhov et al. (2020) detected the equatorward propagating chorus elements and identified the upstream source region. In this study, using Van Allen Probe A data, we investigate the evolution of chorus subpackets. Via the general curvilinear particle-in-cell (gcPIC) simulation model, we further reveal that the nonlinear physics is a dominant process in the evolution of subpackets.

2. Observational Results

2.1. Data Source and Analysis Method

The Van Allen Probes consists of two identical satellites (A and B). The onboard Electric and Magnetic Field Instrument Suite and Integrated Science (EMFISIS, Kletzing et al., 2013) instrument can measure both high-resolution waveform data at 35 kHz and low-resolution triaxial magnetic field data (treated as background magnetic field) at 64 Hz. We perform a fast Fourier transform (FFT) on waveform data to obtain the spectrum. To calculate the instantaneous frequency f, the minimum variance technique is applied to magnetic field data. In this technique, B1 represents the magnetic field component along the maximum variance direction, B2 is the one along the intermediate variance direction, and B3 corresponds to the minimum variance direction (the direction of wave vector $\boldsymbol{k}$). The zero-crossings of B1 are recorded to identify the start and stop times of the half wave cycles, and the f of each half cycle is estimated from the interval between the start and stop times.

2.2. Sweep Rates of Chorus Subpackets in the Upstream and Downstream Regions

Figure 1 shows two chorus elements observed at $L = 5.3$ and MLT = 1.48 in the southern hemisphere with MLAT = −1.8° (the L, MLT, and MLAT values are calculated based on the TS04D model; Tsyganenko & Sitnov, 2005) during 21:26:32.30-:32.70 on 31 March 2013 by Van Allen Probe A, including (a) the spectrum of magnetic field $B^2(=B_1^2 + B_2^2 + B_3^2)$ and (b) the ratio $S_\parallel$/S (where S is Poynting flux and $S_\parallel$ is the parallel component). A value of $S_\parallel$/S ≈ 1 (−1) indicates the forward (backward) propagation along the magnetic field. The two elements are quasi-parallel propagating, with wave normal angles smaller than 20° (not shown). The first element propagates equatorward, so it is observed upstream of the magnetic equator (Nogi & Omura, 2022, 2023). Conversely, the second one propagates poleward, and is in the downstream region.

We select an interval in the upstream region (32.36–32.45 s, marked as T_{up}) and another interval (32.50–32.59 s, marked as T_{down}) in the downstream region to investigate the frequency chirping. The upstream (downstream) waves are filtered in the frequency range of 2.8–3.2 kHz (2.5–3.1 kHz), corresponding to a normalized frequency range of $0.58–0.67\Omega_{e0}$ ($0.52–0.65\Omega_{e0}$), where $\Omega_{e0} = eB_{e0}/m_e$ is the equatorial electron gyrofrequency and B_{e0} is the background magnetic field at the magnetic equator. The temporal evolutions of (c, e) B1 and (d, f) instantaneous frequency f in the T_{up} and T_{down} intervals are also displayed in Figure 1. The T_{up} interval contains two subpackets (#1–#2) with frequency smoothly increasing from ∼2.81 to ∼3.15 kHz. There are five subpackets (#3–#7) in the T_{down} interval, with frequency increasing from ∼2.65 to ∼3.02 kHz. Interestingly, the frequency inside the downstream subpackets does not increase significantly, but remains nearly unchanged. Similar characteristics also appear in the subpackets with the frequency lower than $0.5\Omega_{e0}$ (Supporting information S1).

The upstream and downstream chirpings can be more clearly compared in the zoom-in plots in Figures 1g–1j, where the T_{sub1} and T_{sub5} intervals with a duration of 0.006 s (the shadows in Figures 1c–1f) are shown. The upstream subpacket has a frequency enhancement of ∼0.043 kHz in 0.006 s, corresponding to a sweep rate of

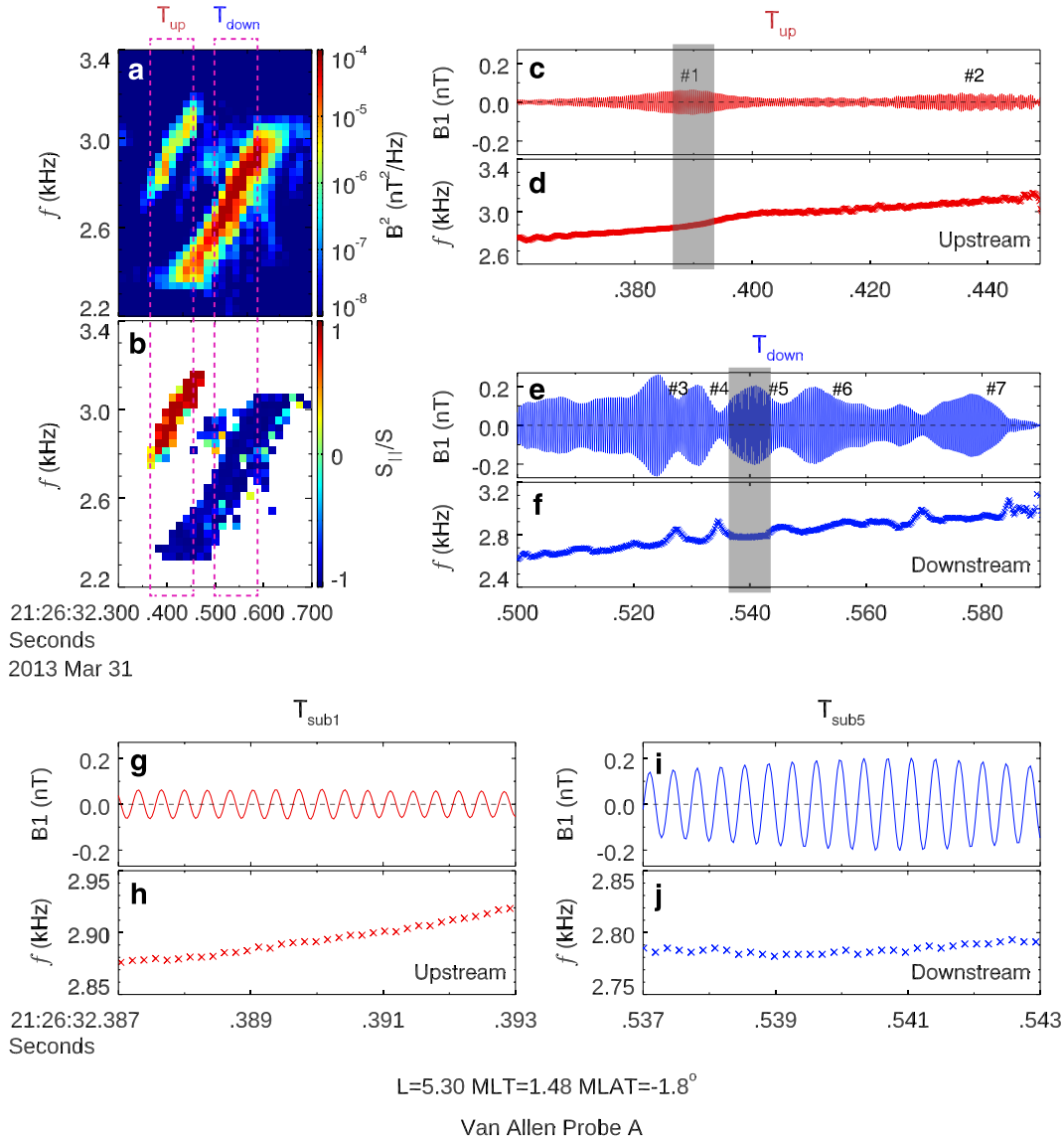

Figure 1. (a) Spectrum of magnetic field B^2 and (b) $S_{\|}/S$ of two chorus elements, with two intervals (T_{up} in the upstream region and T_{down} in the downstream region) denoted by magenta dashed boxes. The time histories of (c, e) B1 and (d, f) instantaneous frequency f in the two intervals. The 0.006-s intervals (marked by shadows) of (g, i) B1 and (h, j) f in the upstream and downstream subpackets. In panels (c–j), the red (blue) color represents the upstream (downstream) subpackets. In panels (c, e), the subpackets are labeled as "#1" to "#7." In panels (g, i), the dashed lines denote $B1 = 0$.

$\Gamma = 7.16$ kHz/s ($=4.98 \times 10^{-5}\Omega_{e0}^2$). While the sweep rate of the downstream subpacket is quite small, with only $\Gamma = 1.28$ kHz/s ($=0.89 \times 10^{-5}\Omega_{e0}^2$). Other subpackets exhibit a similar trend of chirping, except that the subpacket #4 has a slight frequency decrease. Therefore, the sweep rate of the upstream subpackets is generally larger than that of the downstream subpackets.

3. The gcPIC Simulation in the Real-Size Magnetosphere

3.1. Simulation Model and Initial Setup

To investigate the evolution of the subpackets from the upstream to downstream regions, we perform a one-dimensional (1-D) gcPIC simulation in the dipole field. The simulation domain is along the field line, and the reflecting and absorbing boundary conditions are used for particles and waves, respectively. The cold electrons

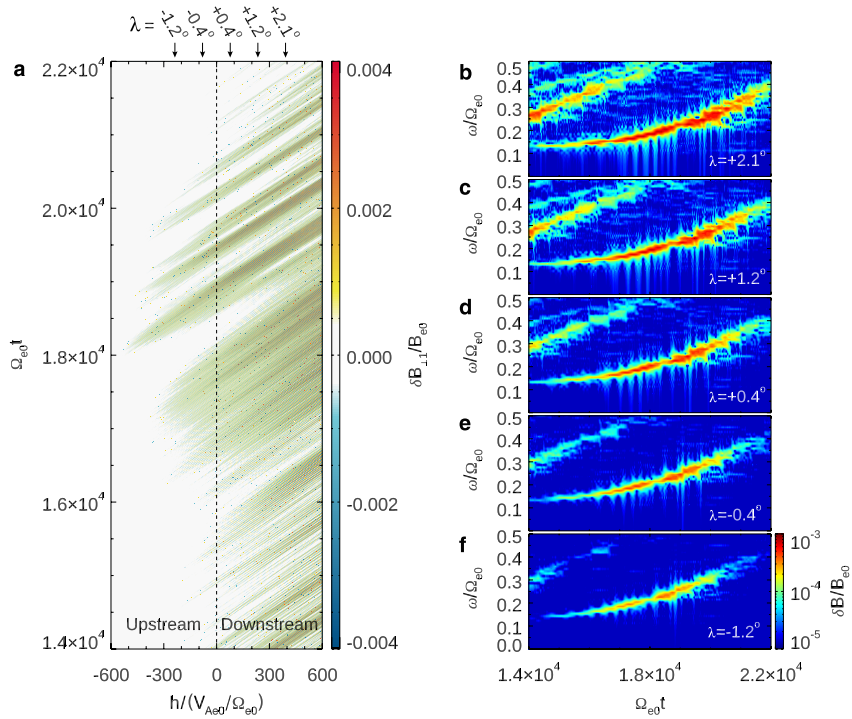

Figure 2. (a) The perpendicular component of wave magnetic field $\delta B_{\perp 1}$ in the h-t plane. The dashed line at $h = 0$ denotes the magnetic equator, and the arrows mark five latitudes ($\lambda = -1.2°$, $-0.4°$, $0.4°$, $1.2°$, and $2.1°$). (b–f) The ω-t spectrum of $\delta B/B_{e0}$ at each latitude.

satisfy a Maxwellian distribution. The energetic electrons are modeled using a subtracted Maxwellian distribution (Omura, 2021), and the distribution function at the magnetic equator is:

$$f(u_{\parallel}, u_{\perp}) = \frac{n_{heq}}{(2\pi)^{3/2} U_{t\parallel} U_{t\perp}^2 (1 - \rho\beta)} \exp\left(-\frac{u_{\parallel}^2}{2U_{t\parallel}^2}\right) \cdot \left[exp\left(-\frac{u_{\perp}^2}{2U_{t\perp}^2}\right) - \rho \exp\left(-\frac{u_{\perp}^2}{2\beta U_{t\perp}^2}\right)\right] \quad (1)$$

where $\rho = 1$ and $\beta = 0.3$, $v_{\parallel}$ and $v_{\perp}$ are the parallel and perpendicular velocities, $U_{t\parallel}$ and $U_{t\perp}$ are the parallel and perpendicular thermal momentums, $u = \gamma v$ is the momentum with the Lorentz factor $\gamma = \left(1 - v^2/c^2\right)^{-1/2}$, and n_{heq} is the number density of energetic electrons at the magnetic equator. Ions are assumed to be immobile. At the magnetic equator, the ratio between the plasma frequency and the electron gyrofrequency is $\omega_{pe}/\Omega_{e0} = 5.0$ ($\omega_{pe} = \sqrt{n_{e0}e^2/m_e\varepsilon_0}$, with ε_0 being the vacuum permittivity and n_{e0} being the number density of cold electrons, which are uniformly distributed), and the initial number density, parallel thermal momentum, and temperature anisotropy of energetic electrons are $n_{heq}/n_{e0} = 0.0016$, $U_{t\parallel}/V_{Ae0} = 0.984$ ($V_{Ae0} = B_{e0}/\sqrt{\mu_0 n_{e0} m_e}$ with μ_0 being the vacuum permeability), and $U_{t\perp}^2/U_{t\parallel}^2 = 3$. Other parameters along the field line can be obtained by using the Liouville's theorem (Summers et al., 2012). The topology of magnetic field at $L = 4$ has been used, and the simulation domain contains 14,400 grids (with a grid length of $0.18V_{Ae0}/\Omega_{e0}$) over the latitudinal range from $-7°$ to $7°$. There are 12,000 particles in each grid for each species. The time step is $\Delta t = 0.03\ \Omega_e^{-1}$.

3.2. Evolution of Chorus Subpackets

Both forward and backward chorus waves are self-consistently excited by energetic electrons. We only study the forward waves because the results in the other direction are similar. Figure 2a shows the perpendicular component of wave magnetic field $\delta B_{\perp 1}$ in the h-t plane, where h is the distance along field line from the magnetic equator, with positive/negative values in the northern/southern hemisphere. For the forward waves, the southern (northern) hemisphere is the upstream (downstream) region. The stripe profiles extending from upstream to downstream represent subpackets, which are first excited upstream with relatively smaller amplitudes ($\delta B/B_{e0}$~0.001, with $\delta B = \sqrt{\delta B_{\perp 1}^2 + \delta B_{\perp 2}^2}$). Then the subpackets propagate downstream, and their amplitudes become larger

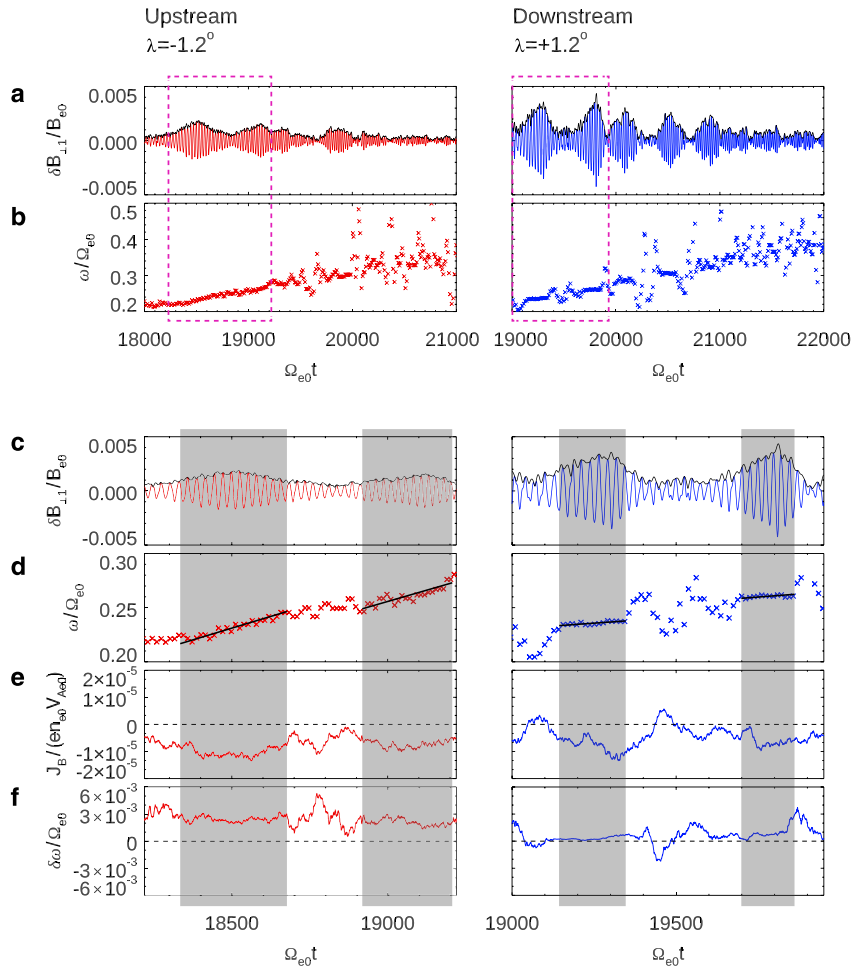

Figure 3. Temporal evolutions of (a) $\delta B_{\perp 1}$ (red or blue lines) and δB (black lines), and (b) instantaneous frequency ω, where the first two subpackets are marked by magenta dashed boxes. Zoom-in plots of (c) $\delta B_{\perp 1}$ and δB, (d) ω, (e) resonant current J_B, and (f) theoretical frequency variation $\delta\omega$ of the two subpackets. The subpackets with large amplitudes are highlighted by gray shadows. In panel (d), the black lines denote the fitting values of ω, and the dashed lines in panels (e, f) represent $J_B = 0$ or $\delta\omega = 0$. The left (right) column is for the upstream (downstream) subpackets, colored in red (blue).

($\delta B/B_{e0}$~0.004). We select five latitudes ($\lambda = -1.2^{\circ}$, -0.4°, 0.4°, 1.2°, and 2.1°), and show the corresponding spectra of δB in Figures 2b–2f. The spectrum at each latitude exhibits a rising tone structure consisting of subpackets. The amplitude and the sweep rate of chorus waves are $\delta B/B_{e0} \sim 10^{-3}$ and $\Gamma \equiv \partial\omega/\partial t \sim 10^{-5}\Omega_{e0}^2$, which are typical values in the magnetosphere (Gao et al., 2022; Li et al., 2009; Teng et al., 2017).

We next compare the upstream and downstream subpackets. Figure 3 shows the temporal evolutions of (a) $\delta B_{\perp 1}$ (red or blue lines) and δB (black lines), and (b) instantaneous frequency ω of the same subpackets at $\lambda = -1.2°$ (in the upstream region) and at $\lambda = 1.2°$ (in the downstream region). To decrease background noises, only the frequencies with $\delta B/B_{e0} > 0.0003$ are shown. The frequency of chorus waves in both upstream and downstream regions increases from ~$0.2\Omega_{e0}$ to ~$0.4\Omega_{e0}$. However, the frequency chirpings in subpackets are different: the upstream subpackets exhibit a smooth increase in frequency, while the downstream subpackets, especially those with large amplitudes, maintain a nearly unchanged frequency. Although there may be frequency decrease between the adjacent subpackets, the overall trend still increases. These chirping characteristics match well with those in observations (Figure 1).

The zoom-in plots of the first two subpackets (marked by the magenta dashed boxes in Figures 3a and 3b) are shown in Figures 3c–3f, including the temporal evolutions of (c) $\delta B_{\perp 1}$ and δB, (d) ω, (e) the resonant current parallel to the wave magnetic field J_B, and (f) the theoretical frequency variation $\delta\omega$. J_B is defined as:

$$J_B = \int_0^{\infty}\int_0^{2\pi}\int_{-\infty}^{\infty}\left[-e\overrightarrow{v_{\perp}}\cdot\delta\hat{\boldsymbol{B}}\right]f(u_{\parallel},\zeta,u_{\perp})u_{\perp}du_{\parallel}d\zeta du_{\perp} \quad (2)$$

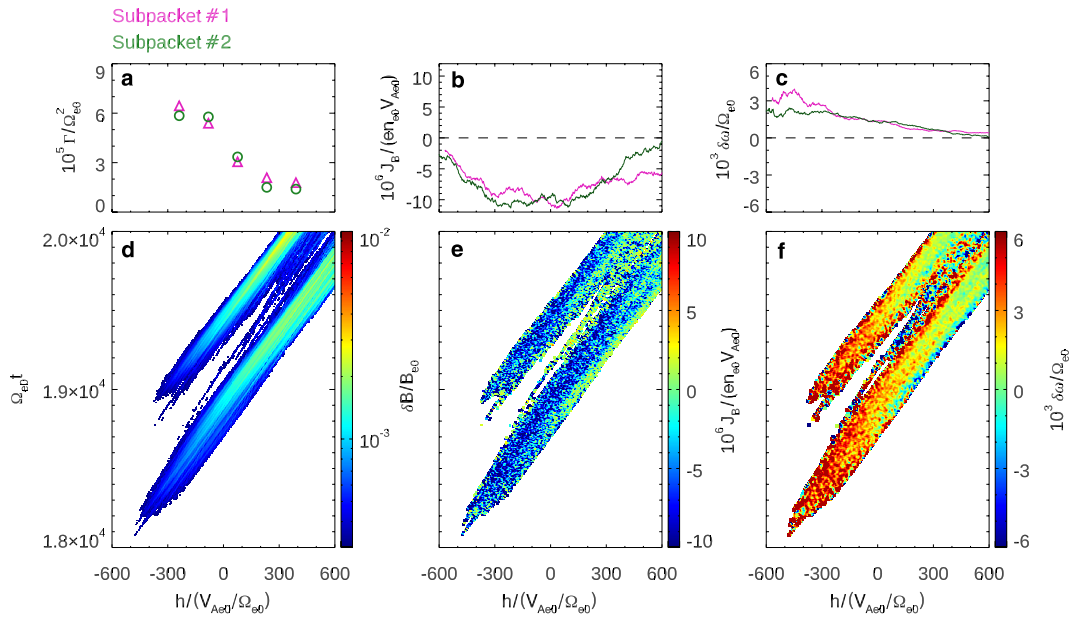

Figure 4. (a) Sweep rate Γ of the first two subpacket at five latitudes. (b) J_B and (c) $\delta\omega$ at the center of subpacket as a function of distance h. In panel (a–c), the magenta (green) color represents the subpacket #1 (#2), and the dashed lines in panels (b, c) denote $J_B = 0$ or $\delta\omega = 0$. (d) δB, (e) J_B, and (f) $\delta\omega$ of the first two subpackets in the h-t plane.

where $\delta\hat{B}$ is the unit vector of the wave magnetic field, and $f(u_{\parallel}, \zeta, u_{\perp})$ is the electron phase space density. The quantity $\delta\omega$ is positively correlated with the sweep rate Γ (Omura, 2021), and is defined as

$$\delta\omega = -\frac{\mu_0 v_g J_B}{2\delta B} \tag{3}$$

where v_g is the group velocity. The shadows mark the intervals with amplitudes greater than 50% of the peak amplitude in each subpacket. In Figure 3d, the different frequency chirpings between the upstream and downstream subpackets are more evident. Using a linear fit (black line), we estimate the sweep rate Γ for the two subpackets: $6.4 \times 10^{-5}\Omega_{e0}^2$ and $5.8 \times 10^{-5}\Omega_{e0}^2$ in the upstream region, and $2.1 \times 10^{-5}\Omega_{e0}^2$ and $1.5 \times 10^{-5}\Omega_{e0}^2$ in the downstream region. According to the nonlinear theory (Omura, 2021; Omura et al., 2008), the sign of J_B determines the chirping direction, with a negative (positive) J_B corresponding to a frequency increase (decrease). In the upstream region (Figure 3e), J_B is always negative, indicating a frequency increase. In the downstream region, apart from the positive values around $\Omega_{e0}t$ = 19,100 and 19,450 when the amplitudes are small, J_B is also negative. Figure 3f shows under large amplitudes (gray shadows), $\delta\omega$ is positive ($\delta\omega/\Omega_{e0} \sim 10^{-3}$) in the upstream region, while it is close to zero but remains positive in the downstream region. Consequently, the theoretical $\delta\omega$ is consistent with the frequency chirping of subpackets in both upstream and downstream regions.

Figure 4a shows the sweep rate Γ of the first two subpackets (#1 in magenta and #2 in green) as a function of distance h, where Γ is estimated using the linear fit (Figure 3d). As expected, the upstream Γ ($\sim 6 \times 10^{-5}\Omega_{e0}^2$) is greater than the downstream one ($\sim 2 \times 10^{-5}\Omega_{e0}^2$). We then extract the waveforms of the two subpackets and display the corresponding (d) δB, (e) J_B, and (f) $\delta\omega$ in the h-t plane. We also identify the propagating trajectory of the center (the wave mode with the largest amplitude) in each subpacket, and plot the evolutions of (b) J_B and (c) $\delta\omega$. In Figure 4d, the amplitude becomes larger during the evolution of subpackets. At the center of subpackets, the quantities J_B ($\sim -10^{-5} e n_{e0} V_{Ae0}$) in the upstream and downstream regions near the magnetic equator are comparable (Figure 4e), which is further illustrated in the line plots in Figure 4b. In Figures 4c and 4f, the upstream $\delta\omega$ is greater than the downstream one, which matches well with the chirping characteristics of subpackets (Figure 3b). Under the condition of J_B being comparable in the upstream and downstream regions, the decrease of $\delta\omega$ downstream is attributed to the larger δB, as depicted in Equation 3. At the edge of subpackets, the quantities J_B and $\delta\omega$ are heavily affected by noise signals due to the small amplitudes.

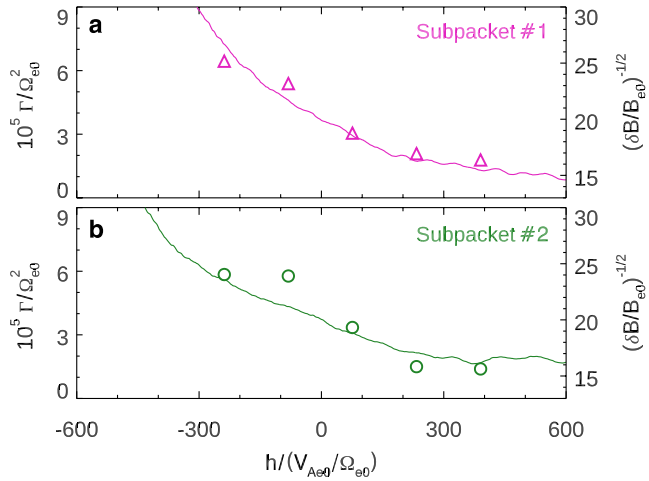

Figure 5. Sweep rate Γ (triangles or circles) and $\delta B^{-1/2}$ (solid lines) as a function of h for subpackets (a) #1 and (b) #2. Subpacket #1 is in magenta and #2 is in green.

4. Discussion

Recently, Nogi and Omura (2022, 2023) proposed the upstream source region of subpackets, as the sum of electron resonance velocity and wave group velocity points upstream and the resonant current is subsequently carried upstream. Through Van Allen Probe A data, we have observed such an upstream source region, where the waves are equatorward propagating along field lines (with wave normal angles smaller than 20°), and their spectrum is relatively weaker than that of downstream waves. Note that the equatorward propagating waves are unlikely to be magnetospherically reflected from higher latitudes, since the reflected waves are typically highly oblique (L. Chen et al., 2013) and their spectrum is at least two orders of magnitude weaker than that of the equatorial waves (Bortnik et al., 2006; Li et al., 2013).

Tsurutani et al. (2020) and R. Chen et al. (2022) reported the nearly unchanged frequency of the intense subpackets inside rising tone elements. In the present study, we find that the subpackets with large amplitudes and low sweep rates are in the downstream region, supported by both observational evidence (Figure 1) and simulation results (Figure 3). Based on the nonlinear theory (Omura, 2021), the frequency variation $\delta\omega$ and the sweep rate Γ satisfy the following relationship:

$$\frac{\delta\omega}{T_N} = \Gamma, \tag{4}$$

where T_N is the nonlinear transition time. There is a parameter τ defined as:

$$\tau = \frac{T_N}{T_{tr}}, \tag{5}$$

where T_{tr} is the trapping time in the subpacket given by:

$$T_{tr} = \frac{2\pi}{\omega_{tr}} = \frac{2\pi}{\chi}\left(\frac{m_e\gamma}{kv_\perp e\delta B}\right)^{1/2}, \tag{6}$$

with $\omega_{tr} = \chi\left[kv_\perp e\delta B/(m_e\gamma)\right]^{1/2}$ and $\chi = 1 - \omega^2/(k^2c^2)$. Assuming τ to be a constant, we have:

$$T_N \propto \delta B^{-1/2}. \tag{7}$$

By substituting Equations 3 and 7 into 4, we obtain:

$$\Gamma \propto \frac{|J_B|}{\delta B^{1/2}}. \tag{8}$$

In our simulation, the resonant currents $|J_B|$ are comparable in the upstream and downstream regions near the magnetic equator (Figure 4b). Consequently, the sweep rate Γ should be negatively correlated with $\delta B^{1/2}$. Figure 5 illustrates Γ and $\delta B^{-1/2}$ as a function of distance h for subpackets (a) #1 and (b) #2 in simulation. The trends in variation between Γ and $\delta B^{-1/2}$ are consistent, confirming the negative correlation between Γ and $\delta B^{1/2}$. However, a positive correlation between $|J_B|$ and $\delta B^{-1/2}$ has been proposed by Omura (2021) (see Equations 82 and 83 in the paper). We have checked the simulation data and found that this positive correlation is valid in the early stage of the subpacket evolution when δB is quite small. As δB increases (e.g., $\delta B/B_{e0} \sim 0.001$) in the subpackets, J_B is found to saturate. When the wave amplitude is large, more electrons are trapped within the wave fields, and the contributing J_B is locked to wave phases, resulting in a minor frequency shift. Conversely, when the amplitude is small, electrons become untrapped, causing a rapid phase spiral between J_B and δB and a more pronounced frequency shift. In the downstream region, the frequency shift primarily occurs between the adjacent subpackets where wave amplitude is small.

Vomvoridis et al. (1982) suggested that the quantity Γ should be positively correlated with $\delta B^{1/2}$ to maximum the nonlinear growth rate. Based on satellite observations, Cully et al. (2011) proposed that this correlation is suitable

for chorus elements. In our simulation, the positive correlation between Γ of chorus elements and $\delta B^{1/2}$ still persists (not shown). Nevertheless, this correlation may vary for chorus subpackets. Between adjacent subpackets, there are frequency irregularities (Figures 1f and 3b), which could be due to the group velocity dispersion during propagation (Hanzelka & Santolík, 2022; Wait, 1965).

Most simulations investigating chorus waves are performed in a parabolic field (Katoh & Omura, 2011; Nogi & Omura, 2022, 2023; Wu et al., 2020), or in a reduced spatial domain (Lu et al., 2019; Ke et al., 2020; H. Chen et al., 2022, 2023a). The typical values of the sweep rate and the element duration (time span of frequency chirping) in these simulations are $\sim 10^{-4}$–$10^{-3}\Omega_{e0}^2$ and $<2000\ \Omega_{e0}^{-1}$, respectively. In contrast, our simulation is conducted in the real-size magnetosphere with the field line topology at $L = 4$, and the sweep rate and the element duration are $\sim 10^{-5}\Omega_{e0}^2$ and $\sim 8000\ \Omega_{e0}^{-1}$, respectively, which are consistent with the observational values ($\sim 10^{-5}\Omega_{e0}^2$ and $\sim 10{,}000\ \Omega_{e0}^{-1}$ in Teng et al. (2017)). Furthermore, the simulated wave spectrum contains subpackets with the time scale of $\sim 500\ \Omega_{e0}^{-1}$ (~11.4 msec), excellently in agreement with those in observations (~10–100 msec, Santolík et al., 2003; Tsurutani et al., 2009; Zhang et al., 2020a, 2020b; Tsurutani et al., 2020). In the next step, we will study the electron precipitation driven by chorus waves using this model.

5. Conclusions

Based on Van Allen Probe A data, we have investigated the evolution of chorus subpackets. The frequency of the upstream subpackets increases smoothly with time, while that of the downstream subpackets remains almost unchanged. Through a gcPIC simulation in the real-size magnetosphere, we have successfully reproduced these subpackets, and found that the frequency sweep rate Γ is influenced by both resonant current J_B and wave amplitude δB, with Γ increasing with J_B but decreasing with δB. Such a result is consistent with the nonlinear theory. Although the resonant currents J_B in the upstream and downstream regions are comparable, the wave amplitude increases significantly during evolution, leading to lower sweep rate in the downstream region. Our study provides a comprehensive understanding of the nonlinear physics in chorus subpackets.

Data Availability Statement

The data from Van Allen Probes were from https://spdf.gsfc.nasa.gov/pub/data/rbsp/. The data used to produce figures in this manuscript are publicly available at H. Chen et al. (2023b).

Acknowledgments
This work was supported by grants NASA-80NSSC21K1688, NASA-80NSSC21K1679, NSF grant AGS-2131012, and in part, by a grant from the NSF EPSCoR program (OIA-2148653) through the Future Technologies and Enabling Plasma Processes (FTPP) project to Auburn University. The work at UTD was supported by the NASA grant 80NSSC21K1320 and the NSF grant AGS-2225121. We acknowledge the entire Van Allen Probes instrument group.

References

An, X., Van Compernolle, B., Bortnik, J., Thorne, R. M., Chen, L., & Li, W. (2016). Resonant excitation of whistler waves by a helical electron beam. *Geophysical Research Letters*, *43*(6), 2413–2421. https://doi.org/10.1002/2015GL067126

Anderson, K. A., & Milton, D. W. (1964). Balloon observations of X rays in the auroral zone: 3. High time resolution studies. https://doi.org/10.1029/JZ069i021p04457

Bortnik, J., Inan, U. S., & Bell, T. F. (2006). Landau damping and resultant unidirectional propagation of chorus waves. *Geophysical Research Letters*, *33*(3), L03102. https://doi.org/10.1029/2005GL024553

Burtis, W. J., & Helliwell, R. A. (1969). Banded chorus a new type of VLF radiation observed in the magnetosphere by OGO 1 and OGO 3. *Journal of Geophysical Research*, *74*(11), 3002–3010. https://doi.org/10.1029/JA074i011p03002

Chen, H., Lu, Q., Wang, X., Fan, K., Chen, R., & Gao, X. (2022). One-dimensional gcPIC-δf simulation of hooked chorus waves in the Earth's inner magnetosphere. *Geophysical Research Letters*, *49*(4), e2022GL097989. https://doi.org/10.1029/2022GL097989

Chen, H., Wang, X., Chen, L., Omura, Y., Lu, Q., Chen, R., et al. (2023a). Simulation of downward frequency chirping in the rising tone chorus element. *Geophysical Research Letters*, *50*(9), e2023GL103160. https://doi.org/10.1029/2023GL103160

Chen, H., Wang, X., Chen, L., Omura, Y., Xia, Z., Lin, Y., & Tsurutani, B. (2023b). Database of 'Evolution of chorus subpackets in the earth's magnetosphere [Dataset]. Zenodo. https://doi.org/10.5281/zenodo.8190801

Chen, L., Thorne, R. M., Li, W., & Bortnik, J. (2013). Modeling the wave normal distribution of chorus waves. *Journal of Geophysical Research: Space Physics*, *118*(3), 1074–1088. https://doi.org/10.1029/2012JA018343

Chen, R., Tsurutani, B. T., Gao, X., Lu, Q., Chen, H., Lakhina, G. S., & Hajra, R. (2022). The structure and microstructure of rising-tone chorus with frequencies crossing at f ~ 0.5 fce. *Journal of Geophysical Research: Space Physics*, *127*(8), e2022JA030438. https://doi.org/10.1029/2022JA030438

Cully, C. M., Angelopoulos, V., Auster, U., Bonnell, J., & Le Contel, O. (2011). Observational evidence of the generation mechanism for rising-tone chorus. *Geophysical Research Letters*, *38*(1), L01106. https://doi.org/10.1029/2010gl045793

Demekhov, A. G., Taubenschuss, U., Hanzelka, M., & Santolík, O. (2020). Frequency dependence of very low frequency chorus poynting flux in the source region: THEMIS observations and a model. *Geophysical Research Letters*, *47*(6), e2020GL086958. https://doi.org/10.1029/2020GL086958

Gao, X., Chen, R., Lu, Q., Chen, L., Chen, H., & Wang, X. (2022). Observational evidence for the origin of repetitive chorus emissions. *Geophysical Research Letters*, *49*(12), e2022GL099000. https://doi.org/10.1029/2022GL099000

Gao, X., Li, W., Thorne, R. M., Bortnik, J., Angelopoulos, V., Lu, Q., et al. (2014). New evidence for generation mechanisms of discrete and hiss-like whistler mode waves. *Geophysical Research Letters*, *41*(14), 4805–4811. https://doi.org/10.1002/2014GL060707

Goldstein, B. E., & Tsurutani, B. T. (1984). Wave normal directions of chorus near the equatorial source region. *Journal of Geophysical Research*, *89*(A5), 2789–2810. https://doi.org/10.1029/JA089iA05p02789

Hanzelka, M., & Santolík, O. (2022). Effects of field-aligned cold plasma density filaments on the fine structure of chorus. *Geophysical Research Letters*, *49*(24), e2022GL101654. https://doi.org/10.1029/2022GL101654

Hanzelka, M., & Santolík, O. (2023). Theories of growth and propagation of parallel whistler-mode chorus emissions: A review. *Surveys in Geophysics*. https://doi.org/10.1007/s10712-023-09792-x

Helliwell, R. A. (1967). A theory of discrete VLF emissions from the magnetosphere. *Journal of Geophysical Research*, *72*(19), 4773–4790. https://doi.org/10.1029/jz072i019p04773

Horne, R. B., & Thorne, R. M. (1998). Potential waves for relativistic electron scattering and stochastic acceleration during magnetic storms. *Geophysical Research Letters*, *25*(15), 3011–3014. https://doi.org/10.1029/98GL01002

Kataoka, R., Miyoshi, Y., Hampton, D., Ishii, T., & Kozako, H. (2012). Pulsating aurora beyond the ultra-low-frequency range. *Journal of Geophysical Research*, *117*(A8), A08336. https://doi.org/10.1029/2012JA017987

Katoh, Y., & Omura, Y. (2011). Amplitude dependence of frequency sweep rates of whistler mode chorus emissions. *Journal of Geophysical Research*, *116*(A7), A07201. https://doi.org/10.1029/2011JA016496

Kawamura, M., Sakanoi, T., Fukizawa, M., Miyoshi, Y., Hosokawa, K., Tsuchiya, F., et al. (2021). Simultaneous pulsating aurora and microburst observations with ground-based fast auroral imagers and CubeSat FIREBIRD-II. *Geophysical Research Letters*, *48*(18), e2021GL094494. https://doi.org/10.1029/2021GL094494

Ke, Y., Lu, Q., Gao, X., Wang, X., Chen, L., Wang, S., & Wang, S. (2020). Particle-in-cell simulations of characteristics of rising-tone chorus waves in the inner magnetosphere. *Journal of Geophysical Research: Space Physics*, *125*(7), e2020JA027961. https://doi.org/10.1029/2020JA027961

Kletzing, C. A., Kurth, W. S., Acuna, M., MacDowall, R. J., Torbert, R. B., Averkamp, T., et al. (2013). The electric and magnetic field instrument suite and integrated science (EMFISIS) on RBSP. *Space Science Reviews*, *179*(1–4), 127–181. https://doi.org/10.1007/s11214-013-9993-6

Li, W., Bortnik, J., Thorne, R. M., Cully, C. M., Chen, L., Angelopoulos, V., et al. (2013). Characteristics of the Poynting flux and wave normal vectors of whistler-mode waves observed on THEMIS. *Journal of Geophysical Research: Space Physics*, *118*(4), 1461–1471. https://doi.org/10.1002/jgra.50176

Li, W., Thorne, R. M., Angelopoulos, V., Bortnik, J., Cully, C. M., Ni, B., et al. (2009). Global distribution of whistler-mode chorus waves observed on the THEMIS spacecraft. *Geophysical Research Letters*, *36*(9), L09104. https://doi.org/10.1029/2009GL037595

Li, W., Thorne, R. M., Bortnik, J., Shprits, Y. Y., Nishimura, Y., Angelopoulos, V., et al. (2011). Typical properties of rising and falling tone chorus waves. *Geophysical Research Letters*, *38*(14), L14103. https://doi.org/10.1029/2011GL047925

Lu, Q., Chen, L., Wang, X., Gao, X., Lin, Y., & Wang, S. (2021). Repetitive emissions of rising-tone chorus waves in the inner magnetosphere. *Geophysical Research Letters*, *48*(15), e2021GL094979. https://doi.org/10.1029/2021GL094979

Lu, Q., Ke, Y., Wang, X., Liu, K., Gao, X., Chen, L., & Wang, S. (2019). Two-dimensional general curvilinear particle-in-cell (gcPIC) simulation of rising-tone chorus waves in a dipole magnetic field. *Journal of Geophysical Research: Space Physics*, *124*(6), 4157–4167. https://doi.org/10.1029/2019ja026586

Macúšová, E., Santolík, O., Décréau, P., Demekhov, A. G., Nunn, D., Gurnett, D. A., et al. (2010). Observations of the relationship between frequency sweep rates of chorus wave packets and plasma density. *Journal of Geophysical Research*, *115*(A12), A12257. https://doi.org/10.1029/2010JA015468

Miyoshi, Y., Oyama, S., Saito, S., Kurita, S., Fujiwara, H., Kataoka, R., et al. (2015). Energetic electron precipitation associated with pulsating aurora: EISCAT and Van Allen Probes observations. *Journal of Geophysical Research: Space Physics*, *120*(4), 2754–2766. https://doi.org/10.1029/2014JA020690

Miyoshi, Y., Saito, S., Kurita, S., Asamura, K., Hosokawa, K., Sakanoi, T., et al. (2020). Relativistic electron microbursts as high-energy tail of pulsating aurora electrons. *Geophysical Research Letters*, *47*(21), e2020GL090360. https://doi.org/10.1029/2020GL090360

Mourenas, D., Zhang, X.-J., Nunn, D., Artemyev, A. V., Angelopoulos, V., Tsai, E., & Wilkins, C. (2022). Short chorus wave packets: Generation within chorus elements, statistics, and consequences on energetic electron precipitation. *Journal of Geophysical Research: Space Physics*, *127*(5), e2022JA030310. https://doi.org/10.1029/2022JA030310

Nogi, T., & Omura, Y. (2022). Nonlinear signatures of VLF-triggered emissions: A simulation study. *Journal of Geophysical Research: Space Physics*, *127*(1), e2021JA029826. https://doi.org/10.1029/2021JA029826

Nogi, T., & Omura, Y. (2023). Upstream shift of generation region of whistler-mode rising-tone emissions in the magnetosphere. *Journal of Geophysical Research: Space Physics*, *128*(3), e2022JA031024. https://doi.org/10.1029/2022JA031024

Nunn, D. (1974). A self-consistent theory of triggered VLF emissions. *Planetary and Space Science*, *22*(3), 349–378. https://doi.org/10.1016/0032-0633(74)90070-1

Omura, Y. (2021). Nonlinear wave growth theory of whistler-mode chorus and hiss emissions in the magnetosphere. *Earth Planets and Space*, *73*(1), 95. https://doi.org/10.1186/s40623-021-01380-w

Omura, Y., Katoh, Y., & Summers, D. (2008). Theory and simulation of the generation of whistler-mode chorus. *Journal of Geophysical Research*, *113*(A4), A04223. https://doi.org/10.1029/2007JA012622

Ozaki, M., Shiokawa, K., Miyoshi, Y., Hosokawa, K., Oyama, S., Yagitani, S., et al. (2018). Microscopic observations of pulsating aurora associated with chorus element structures: Coordinated Arase satellite-PWING observations. *Geophysical Research Letters*, *45*(22), 12125–12134. https://doi.org/10.1029/2018GL079812

Roux, A., & Pellat, R. (1978). A theory of triggered emissions. *Journal of Geophysical Research*, *83*(A4), 1433–1441. https://doi.org/10.1029/JA083iA04p01433

Santolík, O., Gurnett, D. A., Pickett, J. S., Parrot, M., & Cornilleau-Wehrlin, N. (2003). Spatio-temporal structure of storm-time chorus. *Journal of Geophysical Research*, *108*(A7), 1278. https://doi.org/10.1029/2002JA009791

Summers, D., Omura, Y., Miyashita, Y., & Lee, D. H. (2012). Nonlinear spatiotemporal evolution of whistler mode chorus waves in Earth's inner magnetosphere. *Journal of Geophysical Research*, *117*(A9), A09206. https://doi.org/10.1029/2012ja017842

Summers, D., Thorne, R. M., & Xiao, F. L. (1998). Relativistic theory of wave-particle resonant diffusion with application to electron acceleration in the magnetosphere. *Journal of Geophysical Research*, *103*(A9), 20487–20500. https://doi.org/10.1029/98JA01740

Tao, X., Li, W., Bortnik, J., Thorne, R. M., & Angelopoulos, V. (2012). Comparison between theory and observation of the frequency sweep rates of equatorial rising tone chorus. *Geophysical Research Letters*, *39*(8), L08106. https://doi.org/10.1029/2012gl051413

Teng, S., Tao, X., Xie, Y., Zonca, F., Chen, L., Fang, W. B., & Wang, S. (2017). Analysis of the duration of rising tone chorus elements. *Geophysical Research Letters*, *44*(24), 12074–12082. https://doi.org/10.1002/2017GL075824

Thorne, R. M., Li, W., Ni, B., Ma, Q., Bortnik, J., Chen, L., et al. (2013). Rapid local acceleration of relativistic radiation-belt electrons by magnetospheric chorus. *Nature*, *504*(7480), 411–414. https://doi.org/10.1038/Nature12889

Thorne, R. M., Ni, B., Tao, X., Horne, R. B., & Meredith, N. P. (2010). Scattering by chorus waves as the dominant cause of diffuse auroral precipitation. *Nature*, *467*(7318), 943–946. https://doi.org/10.1038/nature09467

Tsurutani, B. T., Chen, R., Gao, X., Lu, Q., Pickett, J. S., Lakhina, G. S., et al. (2020). Lower-band "monochromatic" chorus riser subelement/wave packet observations. *Journal of Geophysical Research: Space Physics*, *125*(10), e2020JA028090. https://doi.org/10.1029/2020JA028090

Tsurutani, B. T., & Gonzalez, W. D. (2006). A new perspective of the relationship between substorms and magnetic storms. In M. Duldig, et al. (Eds.), *Advances in geosciences* (p. 25). World Sci.

Tsurutani, B. T., Lakhina, G. S., & Verkhoglyadova, O. P. (2013). Energetic electron (>10 keV) microburst precipitation, ~5-15 s X-ray pulsations, chorus and wave-particle interactions: A review. *Journal of Geophysical Research: Space Physics*, *118*(5), 2296–2312. https://doi.org/10.1002/jgra.50264

Tsurutani, B. T., & Smith, E. J. (1974). Postmidnight chorus: A substorm phenomenon. *Journal of Geophysical Research*, *79*(1), 118–127. https://doi.org/10.1029/JA079i001p00118

Tsurutani, B. T., Verkhoglyadova, O. P., Lakhina, G. S., & Yagitani, S. (2009). Properties of dayside outer zone chorus during HILDCAA events: Loss of energetic electrons. *Journal of Geophysical Research*, *114*(A3), A03207. https://doi.org/10.1029/2008JA013353

Tsyganenko, N. A., & Sitnov, M. I. (2005). Modeling the dynamics of the inner magnetosphere during strong geomagnetic storms. *Journal of Geophysical Research*, *110*(A3), A03208. https://doi.org/10.1029/2004JA010798

Vomvoridis, J. L., Crystal, T. L., & Denavit, J. (1982). Theory and computer simulations of magnetospheric very low frequency emissions. *Journal of Geophysical Research*, *87*(A3), 1473–1489. https://doi.org/10.1029/JA087iA03p01473

Wait, J. R. (1965). Propagation of pulses in dispersive media. *Radio Science*, *69*(11), 1387–1401. https://doi.org/10.6028/jres.069d.150

Wu, Y., Tao, X., Zonca, F., Chen, L., & Wang, S. (2020). Controlling the chirping of chorus waves via magnetic field inhomogeneity. *Geophysical Research Letters*, *47*(10), e2020GL087791. https://doi.org/10.1029/2020GL087791

Zhang, X.-J., Agapitov, O., Artemyev, A. V., Mourenas, D., Angelopoulos, V., Kurth, W. S., et al. (2020b). Phase decoherence within intense chorus wave packets constrains the efficiency of nonlinear resonant electron acceleration. *Geophysical Research Letters*, *47*(20), e2020GL089807. https://doi.org/10.1029/2020GL089807

Zhang, X.-J., Mourenas, D., Artemyev, A. V., Angelopoulos, V., Kurth, W. S., Kletzing, C. A., & Hospodarsky, G. B. (2020a). Rapid frequency variations within intense chorus wave packets. *Geophysical Research Letters*, *47*(15), e2020GL088853. https://doi.org/10.1029/2020GL088853

Zonca, F., Tao, X., & Chen, L. (2022). A theoretical framework of chorus wave excitation. *Journal of Geophysical Research: Space Physics*, *127*(2), e2021JA029760. https://doi.org/10.1029/2021JA029760